Stability Study and Nonlinear Analysis of DC-DC Power Converters with Constant Power Loads at the Fast Timescale

Haimeng Wu, *Member, IEEE*, Volker Pickert, *Member, IEEE,* Mingyao Ma, *Member, IEEE*
Bing Ji *Member, IEEE and Chenming Zhang*

Abstract— **Rapidly growing distributed renewable networks make an increasing demand on various types of power converters to feed different loads. Power converters with constant power load are one typical configuration that can degrade the stability of the power conversion system due to the negative impedance characteristic. This paper presents a nonlinear analysis method using the developed complete-cycle solution matrix method by transforming the original linear time-variant system into a summation of segmented linear time-invariant systems. Thus, the stability of the nonlinear system can be studied using a series of the corresponding state transition matrix and saltation matrix. As this derived matrix contains all the comprehensive information relating to the system's stability, the influence of the constant power load to system's fast-timescale stability in both continuous conduction mode and the discontinuous conduction mode can be fully investigated and analyzed. The phenomena of fast-timescale instability around switching frequency for power converters with a constant power load are observed and investigated numerically. Finally, experimental results have proven the analysis and verified the effectiveness of the developed method.**

Index Terms—**Nonlinear analysis, boost converters, constant power loads, bifurcation, the complete-cycle solution matrix**

I. INTRODUCTION

FACING the rapid exhaustion of fossil fuel and environmental deterioration, renewable power distribution systems based on power electronics converters are becoming increasingly common. They can be commonly found in grid-connected applications such as smart grids and renewable power integration, and the electric power system (EPS), underpinning the electrical propulsion evolution in automotive systems, aircraft and ship applications [1-3]. The fast-expanding EPS feature multi-converter structures, encompassing different downstream converter blocks such as DC-DC and DC-AC converters to feed electrical loads,

whereas they normally manifest the characteristics of a negative impedance as a constant power load (CPL) by tightly regulating their outputs. Consequently, such configuration of power converters with CPL can degrade the stability of the entire system due to this negative impedance characteristic and the corresponding complex dynamic interaction of such systems can lead to instability issues [4]. These issues of CPLs have been widely reported and discussed in various multi-converters power systems, such as LED lighting system [5], DC microgrids and distribution system[6, 7] and Electric vehicle system [8].

In recent years, there has been an incentive to analyze and overcome the potential instability caused by CPL [9-12]. A large amount of research work has been conducted in this context with numerous proposed strategies. Simple and effective passive damping methods have been developed with usage of additional LC fliter[13], whereas these systems can be costly with increased weight. Alternatively, a variety of active damping approaches have been proposed to stabilize the system from the perspective of control by introducing 'virtual components', such as 'virtual inductor'[14], 'virtual resistor'[15] and 'virtual impedance'[16]. Other active stabilization techniques have also been presented to mitigate the instability issues which either applies the small-signal methods based on the state-space averaging models or the large-signal approaches based on the nonlinear models. Specifically, the small-signal analysis methods using state-space averaging models describes the small-signal behavior of the converter system – the behavior linearized around any operating point while being subjected to perturbations [17]. Thus, classical linear analysis tools can then be effectively employed, which are widely used. For example, [18] investigates the system stability of the power converters with CPL in terms of the system transfer functions at different operational modes and control modes (voltage and current mode control). A virtual-impedance based stabilizer is proposed using a comprehensive small-signal model and the criteria of impedance matching to damp the negative impact caused by CPLs in dc microgrids [16]. Besides, the controllability of non-isolated DC-DC converters feeding CPL has also been studied in [19]. Whereas the high-frequency behavior or sampling effects are not considered, which only proves such systems are controllable as switched affine nonlinear systems. Therefore, some effects caused by the nonlinear components are ignored in these approaches, which may jeopardize its validity in some cases [20].

H. Wu, is with the Department of Mathematics, Physics and Electrical Engineering, Northumbria University, and the School of Engineering, Newcastle Uuniversity, Newcastle upon Tyne, United Kingdom (e-mail: Haimeng_wu@outlook.com)

V. Pickert, and C. Zhang are with the School of Engineering, Newcastle University, Newcastle upon Tyne, United Kingdom (e-mail: Volker.pickert@ncl.ac.uk, c.zhang22@newcastle.ac.uk).

M.Ma is with the School of Electrical Engineering and Automation, Hefei University of Technology, Anhui, China. (miyama@hfut.edu.cn)

B.Ji is with the Department of Engineering, University of Leicester, Leicester, United Kingdom (email: Bing.ji@le.ac.uk)

For large-signal analysis techniques, the objectives and a simplified hypothesis of a CPL usually determine the level of the complexity of the models. Large-signal phase plane analysis and Lyapunov-based stability analysis methods are often employed to estimate the domain of attraction of the system operating point. Based on the large-signal models, the local behavior around the operation point and its basin of attraction can be defined [9]. Compared to the small-signal linear methods, these approaches are less intuitive but dependable as far as validity is concerned. A comprehensive investigation on stability analysis approaches for switching-mode power converters has been presented, which mainly summarizes the methods for predicting instabilities in the power converters from the perspective of discrete-time modelling [21].

Based on large-signal analysis methods, numerous control approaches have been presented to stabilize power converters with CPL in various applications [8, 22, 23]. The investigation of a buck converter loaded by a CPL as well as the corresponding design of a feedback strategy has been carried out in the sea and undersea vehicles application [24]. In addition, a phase plane analysis and the attraction region have been presented to demonstrate system stability, and a reduced-order large-signal model for a cascaded step-down system with a CPL is proposed based on Lyapunov stability theory [25, 26]. An adaptive sliding mode control strategy for boost converters with CPL is proposed to improve the system stability using Lyapunov function [27]. The bifurcation phenomena and the stability boundaries of the photovoltaic-battery hybrid system have been investigated in [28]. A circular switching surface technique is proposed to mitigate the instability created by CPLs in electric vehicle systems where tight-speed controllers in the vehicle's traction system and tightly regulated dc–dc converters produces the constant power behavior [8]. Also, both small-signal and large-signal stability criteria have been derived for the analysis of such hybrid power system with a CPL using Jacobian matrix [29].

Despite the large volume of existing research on the stability analysis methods above, most publications study the stability of DC-DC converters based on a conventional resistive load and slow-timescale instability of a CPL to the system. However, nonlinear phenomena such as fast-timescale bifurcation and chaos in the converters with CPL have rarely been reported and studied in literature to date. Also, SiC and GaN downstream power converters will only accelerate this problem due to their superb high-switching frequency capabilities, which make the need of the presented work even more important. To investigate such fast timescale instability issues of power DC-DC converters, a nonlinear analysis technique based on the Monodromy matrix has been developed and applied in the bidirectional and interleaved boost converters with a resistive load [30, 31] whereas this method cannot be directly applied to CPL due to the inherent characteristics of linear time-variant in CPL.

In this paper, a study of fast-timescale stability analysis for power converters with a CPL is demonstrated using a complete-cycle solution matrix, which is developed from the Monodromy matrix. By transforming the original linear time-variant system into a series of segmented linear time-invariant systems, the corresponding state transition matrix and saltation matrix can be obtained to evaluate the influence of the control parameters and load conditions to system stability. The rest of this paper is organized as follows: The characteristics of CPL and the theoretical principle of the proposed method is discussed in Section II. Section III introduces the operation of a boost power converter with a CPL and the calculation of the complete-cycle solution matrix. The investigation of demonstrated nonlinear phenomena and stability analysis is given using numerical results and experimental validation. Section V summarizes the conclusions drawn from the study work.

II. CHARACTERISTICS OF CPLs AND THEORETICAL PRINCIPLES

A. Characteristics of CPLs

In general, various types of loads can be seen in a power electronics system: 1) constant load voltage, where the voltage across the load terminals is constant regardless of load current levels; 2) constant load current, which sinks constant current from the feeder converter and the voltage across the load is determined by the load impedance; 3) constant resistive load, where load voltage and load current change proportionally, resulting in a constant resistive load behaviour and 4) CPL that requires constant power from the feeder converter, permitting the converter voltage and current fluctuations at the terminal.

Fig. 1 shows a diagram of a typical DC-AC inverter system and a controlled DC-DC power conversion system. In this system, when the DC-AC inverter drives a motor to regulate the constant speed tightly, the subsystem of the inverter and motor
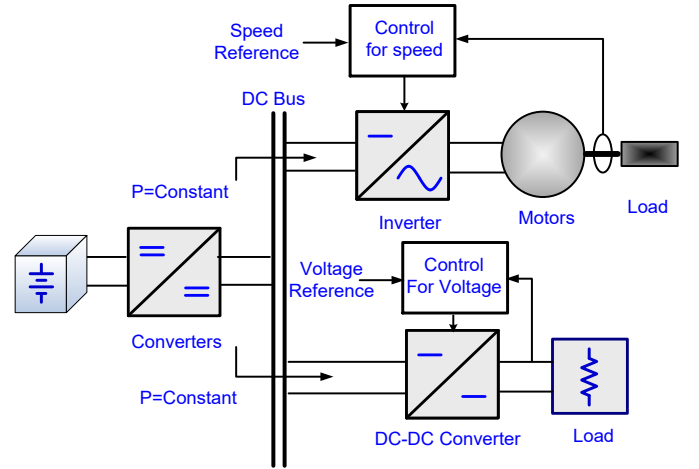

Fig. 1 A typical DC-AC inverter system and a DC-DC power converter using a voltage regulator
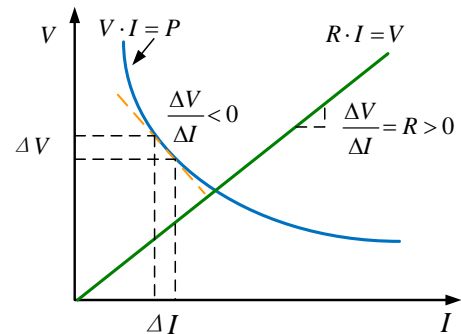

Fig. 2 Characteristics of constant power load and conventional resistive load.

can be regarded as a CPL to the system. CPL can also be found in DC-DC power converters with closed-loop voltage feedback control.

The characteristics of a CPL and a conventional resistive load are demonstrated in Fig. 2. In a CPL, the power is a constant value and can be represented by the product of voltage and the current of the load. Therefore, if the voltage across a CPL is increasing, the corresponding current through it is decreasing and vice versa. In the steady state, the CPL operates at the equilibrium operating point around the output voltage of the feeder converter. This can produce a destabilizing effect on this feeder converter to which the CPL is connected [32]. Specifically, despite the feature of instantaneous positive impedance (V/I > 0), the incremental impedance of CPL is always negative (dV/dI < 0), which is different when compared to the positive impedance of the typical resistive load. This characteristic of negative impedance might affect the stability of distributed power generation systems. Therefore, the classical linear control methods show their limitations on coping with this characteristic of the negative impedance and some effective stabilizing control approaches are proposed to ensure large-signal stability.

B. Proposed Method Developed From Monodromy Matrix

To investigate the fast-timescale instability of power converters with CPL, the Monodromy matrix-based approached is introduced and the basic concept of this method is to determine the stability of the periodic solution by linearizing the system around the whole periodic orbit rather than equilibrium points. This method is developed from the theory of Fillipov that gives a generalized definition of system solutions containing switching behavior[33]. The state transition matrices have been utilized to describe the evolution of the variables before and after each switching action, and the saltation matrix has been employed to express the change of variables during switching action. The system can be proved to be stable if the given initial perturbation $\Delta \mathbf{X}(t_0)$ at t_0 tends to zero when the time t is approaching infinite. Assuming there is a matrix $\Phi(T + t_0, t_0)$ that represents the state transition matrix (STM) of the perturbation over a whole period T. DC-DC switching converters are toggled among subintervals in a complete cycle. For each subinterval, state variables evolve continuously in a smooth trajectory, and thus the system is regarded as linear time-invariant (LTI), and the corresponding solution of STM is shown as:

$$\mathbf{\Phi}(t_1, t_2) = e^{\mathbf{A}(t-t_0)} \tag{1}$$

Because most power electronics systems are piecewise smooth and the vector field is discontinuous at the switching instant, the STM cannot be utilized directly for stability analysis. Thus, to describe the behavior of vector field at switching instants, the saltation matrix S is utilized and its expression can be found in [34, 35]:

$$\mathbf{S} = \mathbf{I} + \frac{(\mathbf{f}_+ - \mathbf{f}_-)\mathbf{n}^T}{\mathbf{n}^T \mathbf{f}_- + \frac{\partial h}{\partial t}} \tag{2}$$

where $\mathbf{I}$ is the identity matrix of the same order of state variables; h defines the switching condition; $\mathbf{n}$ represents the normal vector to the switching and $\mathbf{n}^T$ is its transpose form; $\mathbf{f}_-$ and $\mathbf{f}_+$ are vector fields before and after the switching instant respectively. By implementing the STM before and after the switching instants and saltation matrix, the fundamental solution of a periodic system for one complete cycle can be obtained, which is called as the Monodromy matrix. The stability of the system can be investigated by the magnitudes of the eigenvalue of this matrix [36].

Power DC-DC converters with resistive loads is a nonlinear system that can be described as an LTI system when the switch is in the on and off state. However, for power converters powering a CPL, the state matrices are not independent of time, and thus it becomes a linear time-variant (LTV) system. Because of the nonlinear characteristics of CPL, the analytical expressions of the state transition matrices cannot always be derived from the differential equations in the closed-form. Therefore, the method based on the Monodromy matrix cannot be directly applied to this type of system. To obtain the STM for an LTV system, the concept of differencing and accumulation has been utilized. Assuming $f'(x)$ is the vector fields of the original system, the following equation can be applied:

$$f'(x)\Big|_0^t = \int_0^t f''(x)dx = \sum_{i=1}^n f'' X(i-1) \cdot x)\Big|_{(i-1)\Delta t}^{i\Delta t}, \Delta t = \frac{t}{n} \tag{3}$$

where $f'' X(i-1)$ is a constant value obtained from the derivative expression $f''(x)$ during the small period time Δt. Thus, the original LTV system can be transformed into a summation of segmented LTI system. As this derived matrix contains all the comprehensive information relating to the system's stability, the influence of the constant power load to system's fast-timescale stability can be fully investigated and analysed. For systems in periodic operation, the eigenvalues of this matrix can be calculated to indicate the stable operational region using the given parameters. The varation of the system parameters can make the location movements of the eigenvalues in a unit circle and if the eigenvalues are closer to the boarder of the unit circle, a less stable operational region is obtained.

III. CALCULATION OF THE COMPLETE-CYCLE SOLUTION MATRIX

A. Operation of A Boost Converter with CPL

A peak-current controlled power DC-DC boost converter with CPL is illustrated in Fig. 3(a). When the converter is in the operation of continuous conduction mode (CCM), it is toggled between two subintervals ① and ② as shown in Fig. 3 (b), and the corresponding key operational waveforms of the output voltage $v_c(t)$, the voltage across inductor $v_L(t)$, the current through inductor $i_L(t)$ and the PWM control signals are illustrated in Fig.4 (a). By contrast, the converter is switched among three subintervals ①, ② and ③ in the discontinuous conduction mode (DCM) and the corresponding key operational waveforms are presented in Fig.4 (b).
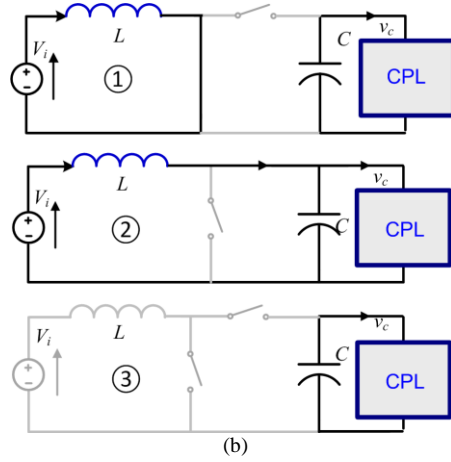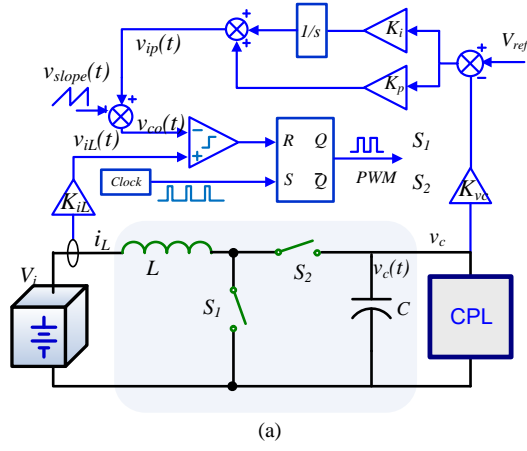
(a)

(b)

Fig. 3 Operation states of a power boost converter with CPLs
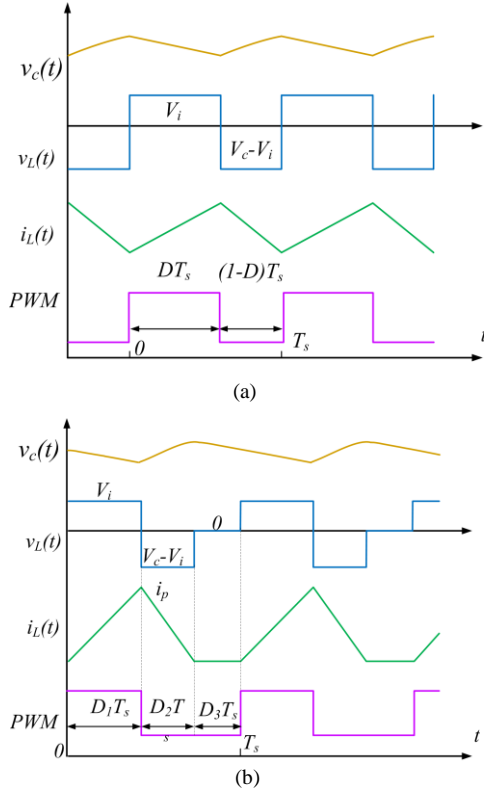

(a)

(b)

Fig.4 Key waveforms of boost converters (a) CCM operation (b) DCM operation

In the controller, K_p and K_i represent the coefficients of the proportion and integrator; K_{vc} and K_{il} are symbols of the gains, which are from the sampled values of output voltage v_c and the inductor current i_L to the signals fed to the controller. Three state vectors x_1, x_2, x_3 are used to represent the capacitor voltage v_c, the inductor current i_L, and the output of the integrator in the feedback loop v_{ip} respectively. The switches S_1 and S_2 are operating complementarily with the PWM control algorithm and thus the corresponding differential equations and the vector fields are given in Table I according to the different operational conditions.

From the equations shown in Table I, the variable v_c is not independent with time t, and the system is defined as a non-homogenous LTV system in the subinterval 2. Thus, there is no analytical solution that can be solved. In order to analyze the system stability using the Monodromy matrix-based approach, the STM must be obtained. Applying (3), the vector fields can be divided into a series of small piecewise subintervals and the trajectory of variables is described by the form of partial differential or the discrete expression, which is presented as follows:

$$-\frac{P}{Cv_c}\Big|_0^{dT} = \int_0^{dT}\frac{P}{Cv_c^2}dv_c = \sum_{i=1}^{n}\frac{P}{CV_{c\_(i-1)}^2}v_c\Big|_{(i-1)\Delta t}^{i\Delta t} \quad (4)$$

Fig.5 illustrates how the varaiables have been represented as a number of pieces in diagram of voltage - cuurent phase potriat in CCM mode. Each interval has been devided into i equal parts, within each small subinterval Δt, the STM can be calculated by

$$\Phi = e^{\mathbf{A}_i(\Delta t)} \quad (5)$$

TABLE I DIFFERENTIAL EQUATIONS AND VECTOR FIELDS AT DIFFERENT SUBINTERVALS

|	Differential equations	Vector fields
Subinterval 1 $0 < t < D_1 T_s$ ①	$\begin{cases}\dfrac{dv_c}{dt} = -\dfrac{P}{Cv_c} \\ \dfrac{di_L}{dt} = \dfrac{V_i}{L} \\ \dfrac{dv_{ip}}{dt} = K_I(V_{ref}-K_{vc}v_c)\end{cases}$ (6)	$f_1 = \begin{bmatrix} -\dfrac{P}{Cx_1} \\ \dfrac{V_i}{L} \\ K_I(V_{ref}-K_{vc}x_1) \end{bmatrix}$ (7)
subinterval 2 $D_1 T < t < (D_1+D_2)T_s$ ②	$\begin{cases}\dfrac{dv_c}{dt} = \dfrac{i_L}{C} - \dfrac{P}{Cv_c} \\ \dfrac{di_L}{dt} = \dfrac{V_i - v_c}{L} \\ \dfrac{dv_{ip}}{dt} = K_I(V_{ref}-K_{vc}v_c)\end{cases}$ (8)	$f_2 = \begin{bmatrix} \dfrac{x_2}{C} - \dfrac{P}{Cx_1} \\ \dfrac{V_i - x_1}{L} \\ K_I(V_{ref} - K_{vc}x_1) \end{bmatrix}$ (9)
subinterval 3 $(D_1+D_2)T_s < t < T_s$ ③	$\begin{cases}\dfrac{dv_c}{dt} = -\dfrac{P}{Cv_c} \\ \dfrac{di_L}{dt} = 0 \\ \dfrac{dv_{ip}}{dt} = K_I(V_{ref}-K_{vc}v_c)\end{cases}$ (10)	$f_3 = \begin{bmatrix} -\dfrac{P}{Cx_1} \\ 0 \\ K_I(V_{ref} - K_{vc}x_1) \end{bmatrix}$ (11)
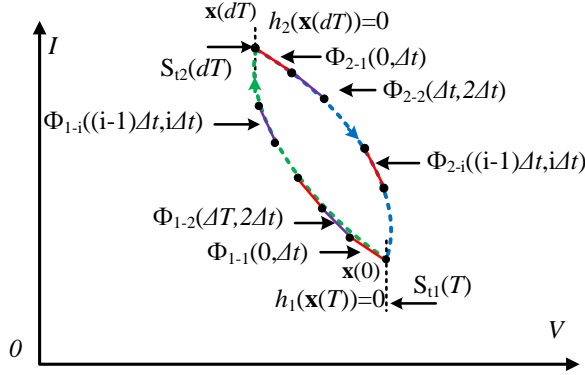
Fig. 5 Concept of the proposed method and corresponding matrices (CCM)

where

$$\mathbf{A}_i = \frac{P}{CV_{c\_(i-1)}^2} \qquad (12)$$

The equations $h_i(x,t)=0$ $(i=1, 2, 3)$ describe the switching conditions and the corresponding Saltation matrices $S_{ti}(i=1, 2, 3)$ represent the evolution of variables the in the switching instants. $V_{c\_(i-1)}$ is a value computed from the last small interval when **I** equals 1, V_{c_0} is the sampled value at the beginning of the switching instant. The following expression is used to calculate the variables analytically.

$$\mathbf{x}\_{(i\Delta t)} = e^{\mathbf{A}_i}\mathbf{x}\_{(i-1)\Delta t} + \int_{(i-1)\Delta t}^{i\Delta t} e^{\mathbf{A}_i}\mathbf{B}\cdot\mathbf{u}\,d\tau \qquad (13)$$
$$= \mathbf{\Phi}_i\mathbf{x}\_{(i-1)\Delta t} + \mathbf{\Psi}_i$$

Therefore, the STM in subintervals 1 and 2, is obtained in the following:

$$\begin{cases} \mathbf{\Phi}_1 = \prod_{i=1}^n \mathbf{\Phi}_{1\_i} \\ \mathbf{\Phi}_2 = \prod_{i=1}^n \mathbf{\Phi}_{2\_i} \end{cases} \qquad (14)$$

If the converter is in DCM mode, the phase portrait of the inductor current and the output voltage is shown as Fig.6. The expression of the STM $\mathbf{\Phi}_1$ and $\mathbf{\Phi}_2$ are same as (14), the experession of $\mathbf{\Phi}_3$ can be obtained by using the equations in subinterval ③. Thus, the corresponding state matrices for each subinterval are shown as follows:
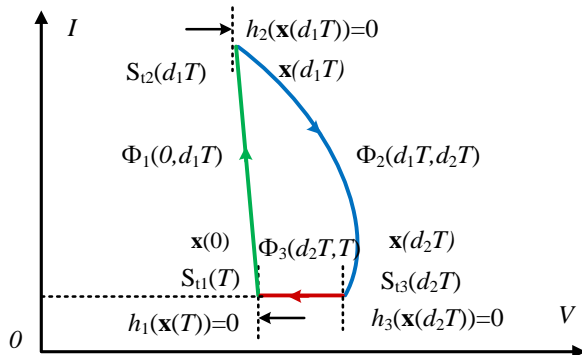

Fig. 6 Phase portrait of inductor current and output voltage (DCM)

$$\mathbf{A}_1 = \mathbf{A}_3 = \begin{bmatrix} \sum_{i=1}^n \frac{P}{CV_{c\_(i-1)}^2} & 0 & 0 \\ 0 & 0 & 0 \\ -K_i K_{vc} & 0 & 0 \end{bmatrix} \qquad (15)$$

$$\mathbf{A}_2 = \begin{bmatrix} \sum_{i=1}^n \frac{P}{CV_{c\_(i-1)}^2} & \frac{1}{C} & 0 \\ -\frac{1}{L} & 0 & 0 \\ -K_i K_{vc} & 0 & 0 \end{bmatrix} \qquad (16)$$

$$\mathbf{B}_1 = \mathbf{B}_2 = \begin{bmatrix} 0 & 0 & 0 \\ 0 & \frac{1}{L} & 0 \\ 0 & 0 & K_I \end{bmatrix} \qquad (17)$$

$$\mathbf{B}_3 = \begin{bmatrix} 0 & 0 & 0 \\ 0 & 0 & 0 \\ 0 & 0 & K_I \end{bmatrix} \qquad (18)$$

$$\mathbf{u} = \begin{bmatrix} 0 \\ V_i \\ V_{ref} \end{bmatrix} \qquad (19)$$

B. Linear Approximation Method

Based on the calculation results of the state transition matrices, the voltage ripple slightly affects the fast-timescale instability of the system, and thus, alternatively, the approximation method of neglecting the output ripple voltage could be employed to transform the original system to the LTI system. The expressions of the approximated linear vector fields and the state matrices for every subinterval are obtained in Table II.

TABLE II

APPROXIMATED DIFFERENTIAL EQUATIONS AND VECTOR FIELDS AT DIFFERENT SUBINTERVALS

$f_1 = \begin{bmatrix} -\dfrac{P}{CV_c} \\ \dfrac{V_i}{L} \\ K_I(V_{ref}-K_{vc}x_1) \end{bmatrix}$	$f_2 = \begin{bmatrix} \dfrac{x_2}{C}-\dfrac{P}{CV_c} \\ \dfrac{V_i-x_1}{L} \\ K_I(V_{ref}-K_{vc}x_1) \end{bmatrix}$	$f_3 = \begin{bmatrix} -\dfrac{P}{CV_c} \\ 0 \\ K_I(V_{ref}-K_{vc}x_1) \end{bmatrix}$
(20)	(21)	(22)

$$\mathbf{A}_1 = \begin{bmatrix} 0 & 0 & 0 \\ 0 & 0 & 0 \\ -K_i K_{vc} & 0 & 0 \end{bmatrix} \quad (23)$$

$$\mathbf{A}_2 = \begin{bmatrix} 0 & \dfrac{1}{C} & 0 \\ -\dfrac{1}{L} & 0 & 0 \\ -K_i K_{vc} & 0 & 0 \end{bmatrix} \quad (24)$$

$$\mathbf{A}_3 = \begin{bmatrix} 0 & 0 & 0 \\ 0 & 0 & 0 \\ -K_i K_{vc} & 0 & 0 \end{bmatrix} \quad (25)$$

$$\mathbf{B}_1 = \mathbf{B}_2 = \begin{bmatrix} -\dfrac{P}{C} & 0 & 0 \\ 0 & \dfrac{1}{L} & 0 \\ 0 & 0 & K_I \end{bmatrix} \quad (26)$$

$$\mathbf{B}_3 = \begin{bmatrix} -\dfrac{P}{C} & 0 & 0 \\ 0 & 0 & 0 \\ 0 & 0 & K_I \end{bmatrix} \quad (27)$$

$$\mathbf{u} = \begin{bmatrix} \dfrac{1}{V_c} \\ V_i \\ V_{ref} \end{bmatrix} \quad (28)$$

Consequently, the characteristic of constant power load can be changed as a constant current load after the approximation.

C. Derivation Of The Complete-Cycle Solution Matrix

For power converters with peak current control, quadratic slope compensation (QSC) method can increase the stable operational region compared with the conventional linear ramp compensation (LRC) [37, 38]. Fig. 7 (a) presents the diagram of the control algorithm for boost converter with CPL, where voltage feedback peak current control with proportional-integral (PI) and QSC method is applied. When the measured inductor current signal v_{iL} is equal to the output of the PI controller v_{con} after signals scaling, an RS flip-flop changes the output state from on to off so that switch S_1 (Fig. 3 (a)) switches accordingly. Fig. 7 (b) shows the illustration of QSC scheme and the corresponding waveforms. The equation $y(t)=-a_m(t/T_s)^2 + V_{con}$ can be used to describe the waveform of the compensation slope in a switching period, where V_{con} equals
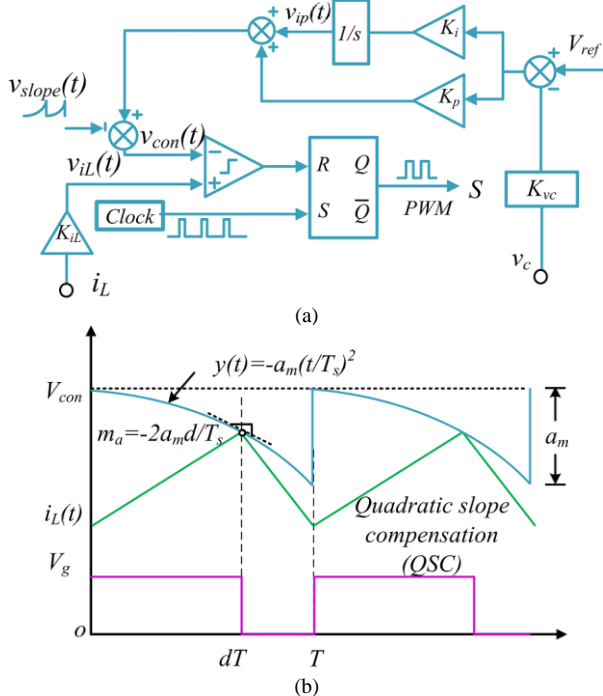

(a)

(b)

Fig. 7 (a) Diagram of the control algorithm for boost converter with CPL (b) Illustration of quadratic slope compensation (QSC) method

$K_p(V_{ref}-K_{vc}x_1)+v_{ip}$. x_1, x_2 and x_3 are utilized to represent the three variables of capacitor voltage v_c, the inductor current i_L, and the output of the integrator in the feedback loop v_{ip}, respectively. The switching condition $h_2(x,t)$ which is related to the action from ON to OFF state can be specified as follows:

$$h_2(x,t) = K_p(V_{ref} - K_{vc}x_1) + x_3 - a_m(t/T)^2 - K_{iL}x_2 \quad (29)$$

Hence, its normal vector can be obtained as:

$$\mathbf{n}_2 = \begin{bmatrix} \partial h_2/\partial x_1 \\ \partial h_2/\partial x_2 \\ \partial h_2/\partial x_3 \end{bmatrix} = \begin{bmatrix} -K_p K_{vc} \\ -K_{iL} \\ 1 \end{bmatrix} \quad (30)$$

And its rate of change is given by:

$$\frac{\partial h}{\partial t} = -\frac{2a_m}{T}t \quad (31)$$

At the switching instant ($t=DT$), the value of this term equals $2a_mD$. The other terms involved in equation (2) can be expressed as follows:

$$(\mathbf{f}_2 - \mathbf{f}_1)\mathbf{n}_2^T = \begin{bmatrix} -\dfrac{K_p K_{vc} x_2}{C} & -\dfrac{K_{iL}x_2}{C} & \dfrac{x_2}{C} \\ \dfrac{K_p K_{vc} x_1}{L} & \dfrac{K_{iL}x_1}{L} & -\dfrac{x_1}{L} \\ 0 & 0 & 0 \end{bmatrix} \quad (32)$$

$$\mathbf{n}_2^T \mathbf{f}_1 = \frac{K_P K_{vc} P}{C x_1} - \frac{K_{iL}V_i}{L} + K_I(V_{ref} - K_{vc}x_1) = s_p \quad (33)$$

Hence the saltation matrix S_{t2} can be obtained as:

$$\mathbf{S}_{t2} = \begin{bmatrix} 1 - \dfrac{K_p K_{vc} x_2}{C(s_p - 2a_m D)} & -\dfrac{K_{iL}x_2}{C(s_p - 2a_m D)} & \dfrac{x_2}{C(s_p - 2a_m D)} \\ \dfrac{K_p K_{vc} x_1}{L(s_p - 2a_m D)} & 1 + \dfrac{K_{iL}x_1}{L(s_p - 2a_m D)} & -\dfrac{x_1}{L(s_p - 2a_m D)} \\ 0 & 0 & 1 \end{bmatrix} \quad (34)$$

As the rising edge of the periodical clock signal causes the term in (2) to be infinite, it makes the corresponding saltation matrix an identity matrix, and thus both the first saltation matrix in CCM and DCM operation are given as identity matrices.

$$\mathbf{S}_{t1} = \mathbf{I} \quad (35)$$

If the third switching function is defined as $h_3(x,t)$, the following is obtained

$$h_3(x,t) = x_2 = 0 \quad (36)$$

Thus:

$$\mathbf{n} = \begin{bmatrix} \partial h_3/\partial x_1 \\ \partial h_3/\partial x_2 \\ \partial h_3/\partial x_3 \end{bmatrix} = \begin{bmatrix} 0 \\ 1 \\ 0 \end{bmatrix} \quad (37)$$

and:

$$\frac{\partial h}{\partial t} = 0 \tag{38}$$

$$(\mathbf{f}_3 - \mathbf{f}_2)\mathbf{n}^T = \begin{bmatrix} -\dfrac{x_2}{C} \\ \dfrac{x_1 - V_i}{L} \\ 0 \end{bmatrix} \begin{bmatrix} 0 & 1 & 0 \end{bmatrix} = \begin{bmatrix} 0 & -\dfrac{x_2}{C} & 0 \\ 0 & \dfrac{x_1 - V_i}{L} & 0 \\ 0 & 0 & 0 \end{bmatrix} \tag{39}$$

$$\mathbf{n}_3^T \mathbf{f}_2 = \begin{bmatrix} 0 & 1 & 0 \end{bmatrix} \begin{bmatrix} \dfrac{x_2}{C} - \dfrac{P}{Cx_1} \\ \dfrac{V_i - x_1}{L} \\ K_I(K_{vc}x_1 - V_{ref}) \end{bmatrix} = \dfrac{V_i - x_1}{L} \tag{40}$$

$$\mathbf{S}_{t3} = \begin{bmatrix} 1 & -\dfrac{x_2 L}{(V_i - x_1)C} & 0 \\ 0 & 0 & 0 \\ 0 & 0 & 1 \end{bmatrix} \tag{41}$$

By applying the following equations, the complete-cycle solution matrix M, which is also the STM of the whole clock period, can be calculated as follows:

$$\begin{cases} \mathbf{M} = \mathbf{S}_{t1} \times \prod_{i=1}^{n} \mathbf{\Phi}_{1\_i} \times \mathbf{S}_{t2} \times \prod_{i=1}^{n} \mathbf{\Phi}_{2\_i} & CCM \\ \mathbf{M} = \mathbf{S}_{t1} \times \prod_{i=1}^{n} \mathbf{\Phi}_{1\_i} \times \mathbf{S}_{t2} \times \prod_{i=1}^{n} \mathbf{\Phi}_{2\_i} \times \mathbf{S}_{t3} \times \prod_{i=1}^{n} \mathbf{\Phi}_{3\_i} & DCM \end{cases} \tag{42}$$

IV. STABILITY ANALYSIS

A. Simulation Verification

TABLE III

SPECIFICATIONS OF SYSTEM PARAMETERS

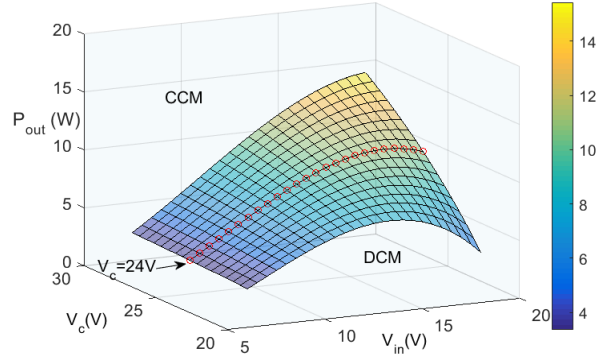| Parameters	Value	Parameters	Value
Input voltage （V）	6~18	Frequency （kHz）	50
Output voltage （V）	24	K_{iL}	1/8.5
Power rating （W）	0-50	K_{p1}	0.5
Inductance （μH）	75	K_{i1}	2000
Output capacitance （μF）	40	K_{vc}	1/3

Fig. 8 boundary power curve of CCM and DCM operation

The power boost circuit with CPL is implemented in Matlab/Simulink using the specifications of parameters given in Table III. In the CCM operation, half of the peak current is less than the average input current in the steady state. With the assumption of the ideal power conversion the following equation must be satisfied for CCM operation:

$$P \geq \frac{V_i^2 (V_c - V_i) T_s}{2 V_c L} \tag{43}$$

Using the parameters given in Table III, the boundary power curve of CCM and DCM operation can be obtained as illustrated in Fig. 8. In the simulation, the CPL is represented by using an embedded Matlab function and a voltage-controlled current source. The instantaneous input voltage V and the given output power P are the inputs of the MATLAB Function block, where the output current can be calculated by the equation of $I = P/V$. This output signal is fed to the block of the voltage-controlled current source to generate an instantaneous load current for the power converter. Fig. 9 shows the bifurcation diagram of a bidirectional boost converter with 25W CPL at different input voltages and a_m in CCM. The bifurcation diagram is a graphical representation method generally used to study nonlinear phenomena. To generate the bifurcation diagram in the simulation, V_{in} and a_m are chosen as two bifurcation parameters with variation of defined steps. The system runs until reaching steady state and the last N periods of output voltage and inductor current (e.g. N=50) are sampled accordingly. Subsequently, this process has been repeated using a different set of the bifurcation parameters to obtain other outcomes. Thus, the 3D bifurcation diagram can be produced in Matlab, where V_{in} and a_m are varied and plotted along x and y axis, and the output voltage and inductor current are and plotted on the Z axis, respectively. The converter can be proved to run in a stable state (period-1), if only one overlapped point is plotted after continuous sampling of the variables (inductor current and capacitor voltage) at switching frequency for a dozen times. Two points can be identified in the diagram when the converter is operating in period-2 (period-doubling bifurcation). Randomly scattered points can be observed when the converter is in a chaotic state.
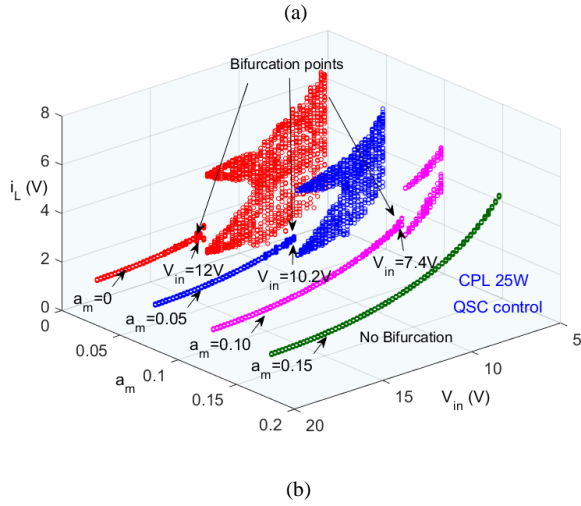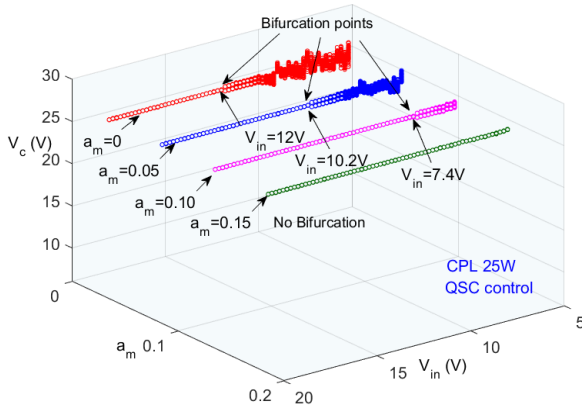
(a)

(b)

Fig. 9 (a) Bifurcation diagram of the boost converter with CPL (25W) at different input voltages and a_m in Simulation: (a) Output voltage (b) Inductor current

To validate the expression of the complete-cycle solution matrix M, the calculated results using analytical expression in Matlab has been checked with the corresponding numerical simulation results using Simulink. The eigenvalue of the matrix can be calculated for each set of given parameters when the system is in stable operation. With the increase of the radius of these eigenvalues (within the unit circle), the system will gradually lose the stable margin and eventually lose stability when the locus of eigenvalues are located on the boarder of unit circle. The corresponding status of the system can be observed using the simulation result.
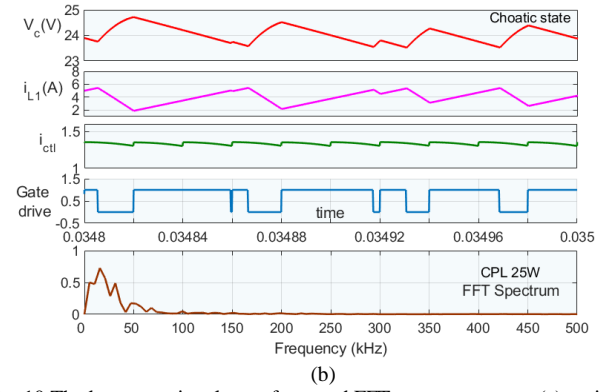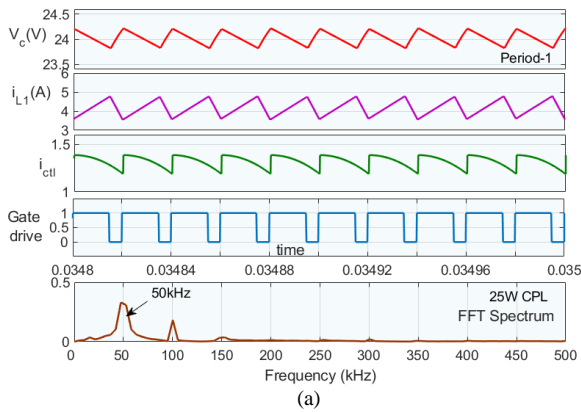

(a)

(b)

Fig. 10 The key operational waveform and FFT power spectrum (a) period-1 (b)chaotic state

It is evident that the stable region of the converter is extended when the amplitude of compensation slope a_m is increased. Specifically, when there is no compensation slope (a_m=0) than V_{in} equals to 12V becoming the bifurcation point; when a_m equals 0.05 and 0.10, the corresponding bifurcation point becomes 10.2V and 7.4V, respectively. In contrast, there is no bifurcation point identified when a_m equals 0.15. Fig. 10 presents two examples of key operational waveforms using different compensation slopes a_m when input voltage equals 6V.The periodic waveform and FFT spectrum at switching frequency of 50kHz demonstrate the converter operates in a stable state in Fig. 10 (a) when a_m=0.15 and the nonperiodic and random-like waveforms show the converter is in a chaotic state as illustrated in Fig. 10 (b) when a_m is reduced to 0.05.

The third-order matrix M can obtain three relevant eigenvalues using the specific parameters. However, However, there is only one eigenvalue plays a dominant role in indicating the period-doubling bifurcation behaviour which relates to the inductor current and the other two eigenvalues have slight changes in the variation of parameters. Fig. 11 shows an example of the locus of the calculated relevant eigenvalues to fast-timescale instability at the variation of input voltage when a_m equals 0.05. The eigenvalue moves to the border of the unit circle along the negative real line when V_{in} is decreased from 18V to 10.2V, which also demonstrates that the system will exhibit the period-doubling bifurcation beyond the point of 10.2V.

To study how load can affect the stability of power converter, Fig. 12 (a) illustrates an example of the influence of the
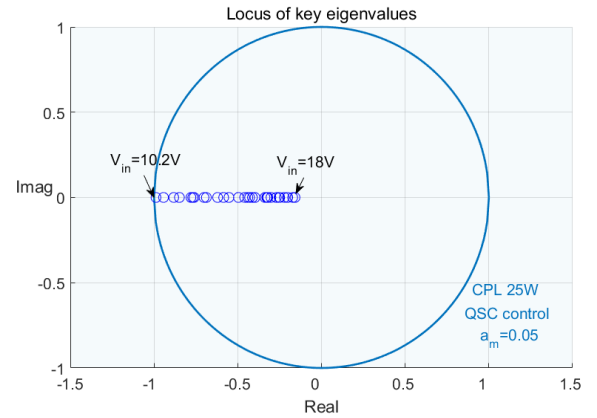

Fig. 11 Locus of relevant eigenvalues when a_m=0.05 (25W CPL)

variation of CPL and a_m to the system's stability when V_{in} equals 8V, it is evident that when a_m is bigger than 0.1, the power converter can be in stable operation at the entire power range from 5 to 50W. Also, when a_m is less than 0.1 with steps of 0.01, the corresponding bifurcation points of a_m and P_{out} can be found using the bifurcation diagram, and the 2nd order polynomial fitting curve is given in Fig. 12 (b). Fig.12 (c) shows the bifurcation diagram of output voltage at different input voltage and output power when a_m equals 0.05. It can be seen that the bifurcation point is about 8.8V (V_{in}) when P_o equals 10 W, whereas the output power has less influence on the bifurcation points when P_o equals 20 to 50 W, respectively, which have bifurcation around 10V.
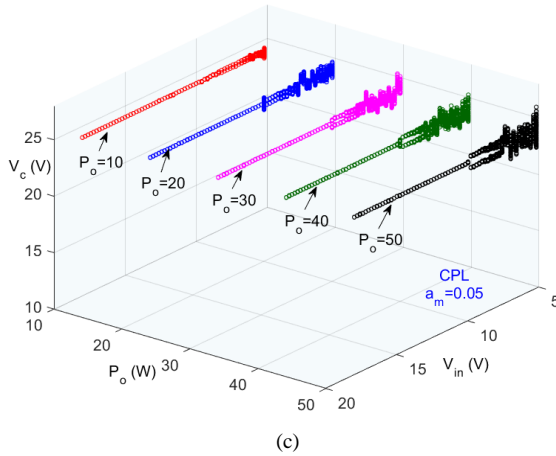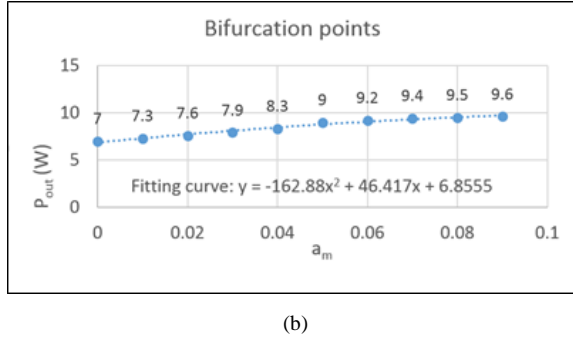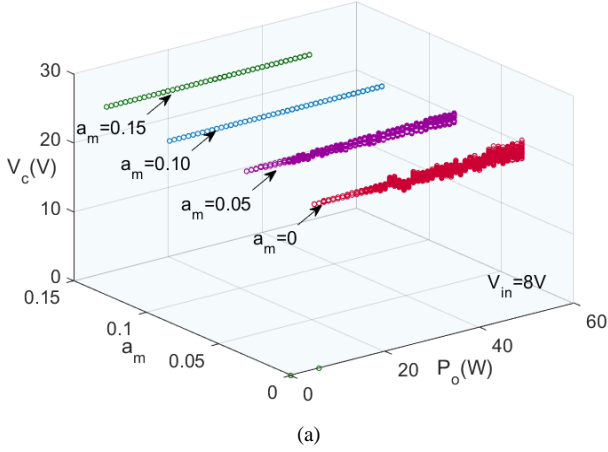
(a)

(b)

(c)

Fig. 12 (a) Influence of output power and a_m to the stability of boost converter with CPL (b) The bifurcation points with corresponding fitting curve (a_m <0.1) (c) Bifurcation diagram of output voltage at different input voltage and output power

B. Experimental Verification

Using the specification given in Table 1, a boost power converter and control circuit has been designed to verify the stability analysis discussed in the simulation section. A programmable DC electronic load, Chroma 63210, is utilized to configure at CPL mode as shown in Fig. 13 (a). To generate the control signal with QSC method, a mixed-signal controller is applied to measure the inductor current i_L and capacitor voltage v_c as well as processing the PI control algorithm, which is illustrated in Fig. 13 (b). Labview with SPI communication has been used to capture and to transfer the measurement data from DSP controller to the computer. The output voltage v_c and inductor current i_L have been sampled once at each switching period. When the power converter is in operation with CPL, there is a control button on the labview panel to execute the consecutive 50 time sampling action. Then the measured data will be stored in the computer to process, generating the experimental bifurcation diagram.

The experimental results of the bifurcation diagram at different input voltages and a_m are shown in Fig. 14. Compared with the simulation results in Fig. 9, both profile and bifurcation are quite close but with some differences in terms of the practical values of a_m employed. Slightly larger values of a_m are required in the experiment to achieve a similar control effect in the simulation. This could be caused by the difference of ideal models used in simulation and parasitic parameters existing in the prototype and the errors produced in the sampling and signal processing circuits. In general, there is a good agreement between the simulation and experiment results, and both prove that the phenomena of fast-timescale instability around switching frequency can take place in the power converter with CPL. Furthermore, the stability of the power converter with CPL regulated by a controller can be
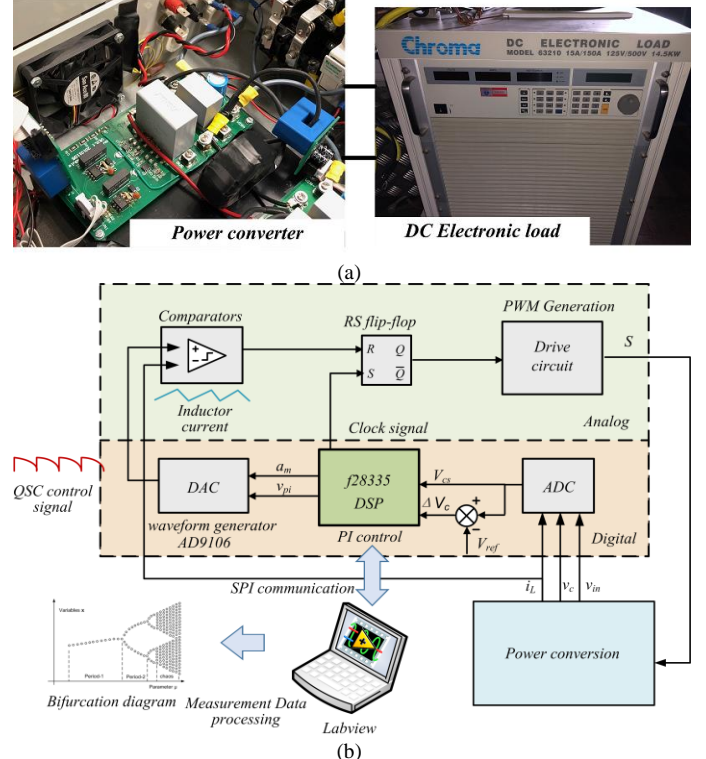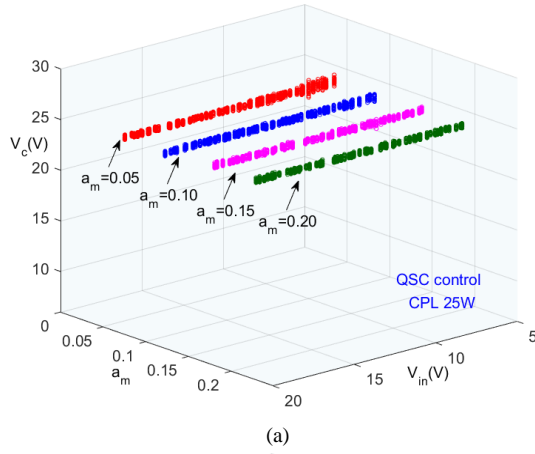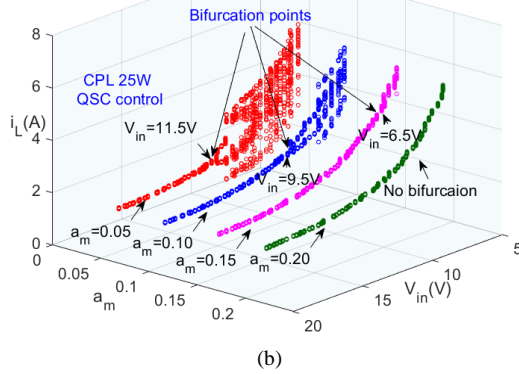
(a)

(b)

Fig. 13 (a) Designed power converter with DC electronic CPL (b) control blocks of the mixed-signal controller

(a)

(b)

Fig. 14 (a) Experimental bifurcation diagram of the boost converter with CPL at different input voltages and a_m (a) output voltage (b) inductor current

investigated by the developed nonlinear analysis method based on the Monodromy matrix.

Fig. 15 demonstrates the experimental results of key operational waveforms at different a_m (0.10, 0.15, 0.20) when V_{in} equals 6V, and the output voltage is 24V. The power converter performs chaotic state (a_m=0.10), period-2 (a_m=0.15), and period-1 stable operation (a_m=0.15), respectively, as shown in Fig. 13 (a), (b), and (c). To further investigate how the power level can affect the performance of the converter, the CPL is set from 5 to 50 W with steps of 1 W. As shown in Fig. 16 (a), the experimental bifurcation diagram of the inductor current is obtained when a_m equals 0.1.
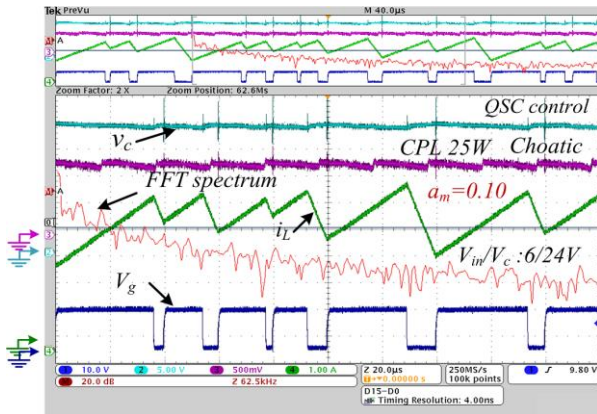

(a)
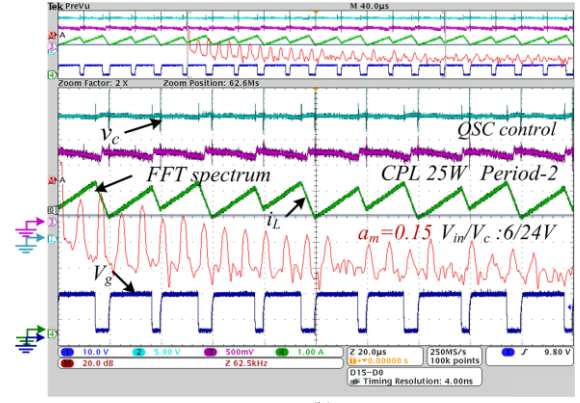
(b)
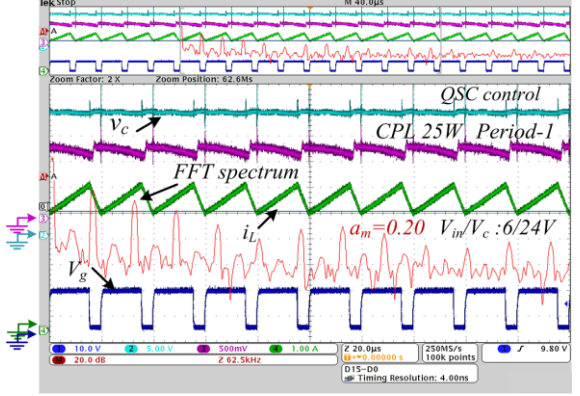
(c)

Fig. 15 Experimental results of key operational waveforms with 25W CPL using QSC control (V_{in}=6V, V_c=24V): (a) a_m=0.10; (b) a_m=0.15; (c) a_m=0.20

Curve 1 presents that bifurcation takes place when the load is 18W, and the input voltage equals 8V, in contrast, Curve 2 is recorded when the input voltage is changed to 12V, the bifurcation phenomena can only be observed when the power load is less than 6 W. Fig. 16 (b) and (c) shows the key operational waveform at 5W and 50W load, respectively when the input voltage equals 12V. It is evident that the converter operates in a doubling period (period-2) state when having the load of 5W. Using the knowledge gained from the stability study of the power converter with CPL as presented in Fig. 12, an advanced controller with appropriate control parameters can be designed to control the stable operation of the power converter in a wide range of load.
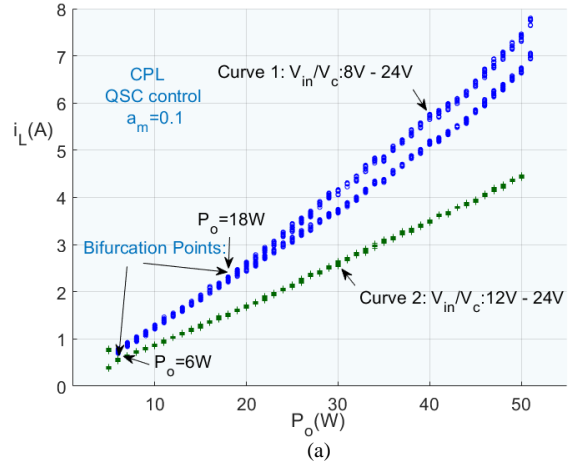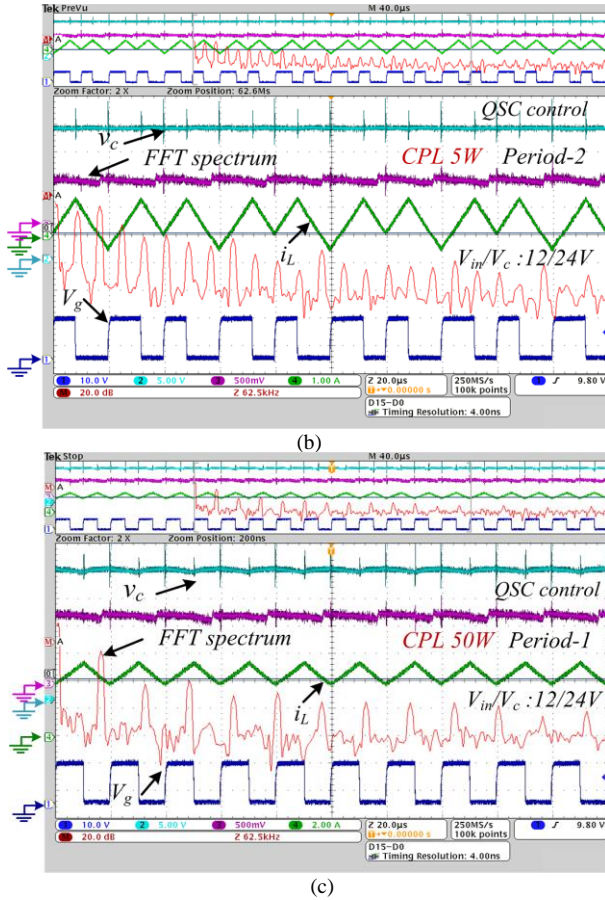

(a)

Fig. 16 (a) Experimental bifurcation diagram of inductor current at the variation of power load (V_{in} equals 8 and 12V) (b) Key operational waveform at 5W, 12V input (c) Key operational waveform at 50W, 12V

V. CONCLUSION

Power boost converters with CPL are identified as an LTV system, which cannot be studied by the classical stability analysis approaches for LTI system. This paper develops a nonlinear analysis method based on the complete-cycle matrix that can be applied to investigate the nonlinearity of the LTV system, introducing the concept of differencing and accumulation to the Monodromy matrix-based approach. In addition, a linear approximation method is proposed to reduce the calculation of the matrix with all the analytical expression given in details. The influence of the characteristics of the CPL on system stability at fast-timescale is fully studied in simulation which is also verified in the experiments. The result shows the effectiveness of this nonlinear analysis approach in the investigation of fast-timescale instability in power converter with CPL.

REFERENCES

[1]   A. Emadi, A. Khaligh, C. H. Rivetta, and G. A. Williamson, "Constant power loads and negative impedance instability in automotive systems: Definition, modeling, stability, and control of power electronic converters and motor drives," (in English), *IEEE Transactions on Vehicular Technology,* vol. 55, no. 4, pp. 1112-1125, Jul 2006.

[2]   A. M. Rahimi and A. Emadi, "An Analytical Investigation of DC/DC Power Electronic Converters With Constant Power Loads in Vehicular Power Systems," *IEEE Transactions on Vehicular Technology,* vol. 58, no. 6, pp. 2689-2702, 2009.

[3]   D. Marx, P. Magne, B. Nahid-Mobarakeh, S. Pierfederici, and B. Davat, "Large Signal Stability Analysis Tools in DC Power Systems With Constant Power Loads and Variable Power Loads: A Review," *IEEE Transactions on Power Electronics,* vol. 27, no. 4, pp. 1773-1787, 2012.

[4]   M. K. Zadeh, R. Gavagsaz-Ghoachani, J.-P. Martin, B. Nahid-Mobarakeh, S. Pierfederici, and M. Molinas, "Discrete-time modeling, stability analysis, and active stabilization of dc distribution systems with multiple constant power loads," *IEEE Transactions on Industry Applications,* vol. 52, no. 6, pp. 4888-4898, 2016.

[5]   M. Gutierrez, P. A. Lindahl, A. Banerjee, and S. B. Leeb, "An Energy Buffer for Controllable Input Impedance of Constant Power Loads," *IEEE Transactions on Industry Applications,* vol. 55, no. 3, pp. 2910-2921, 2019.

[6]   M. A. Hassan, E.-P. Li, X. Li, T. Li, C. Duan, and S. Chi, "Adaptive Passivity-Based Control of DC-DC Buck Power Converter with Constant Power Load in DC Microgrid Systems," *IEEE Journal of Emerging and Selected Topics in Power Electronics,* 2018.

[7]   M. Zhang, Y. Li, F. Liu, L. Luo, Y. Cao, and M. Shahidehpour, "Voltage stability analysis and sliding-mode control method for rectifier in DC systems with constant power loads," *IEEE Journal of Emerging and Selected Topics in Power Electronics,* vol. 5, no. 4, pp. 1621-1630, 2017.

[8]   M. Anun, M. Ordonez, I. G. Zurbriggen, and G. G. Oggier, "Circular switching surface technique: High-performance constant power load stabilization for electric vehicle systems," *IEEE Transactions on Power Electronics,* vol. 30, no. 8, pp. 4560-4572, 2014.

[9]   C. Rivetta and G. A. Williamson, "Global behaviour analysis of a DC-DC boost power converter operating with constant power load," in *Circuits and Systems, 2004. ISCAS '04. Proceedings of the 2004 International Symposium on*, 23-26 May 2004 2004, vol. 5, pp. V-956-V-959 Vol.5.

[10]   P. Liutanakul, A. B. Awan, S. Pierfederici, B. Nahid-Mobarakeh, and F. Meibody-Tabar, "Linear Stabilization of a DC Bus Supplying a Constant Power Load: A General Design Approach," (in English), *IEEE Transactions on Power Electronics,* vol. 25, no. 2, pp. 475-488, Feb 2010.

[11]   A. Kwasinski and C. N. Onwuchekwa, "Dynamic Behavior and Stabilization of DC Microgrids With Instantaneous Constant-Power Loads," (in English), *IEEE Transactions on Power Electronics,* vol. 26, no. 3, pp. 822-834, Mar 2011.

[12]   E. Hossain, R. Perez, A. Nasiri, and S. Padmanaban, "A comprehensive review on constant power loads compensation techniques," *IEEE access,* vol. 6, pp. 33285-33305, 2018.

[13]   M. Cespedes, L. Xing, and J. Sun, "Constant-power load system stabilization by passive damping," *IEEE Transactions on Power Electronics,* vol. 26, no. 7, pp. 1832-1836, 2011.

[14]   S. Liu, P. Su, and L. Zhang, "A virtual negative inductor stabilizing strategy for DC microgrid with constant power loads," *IEEE Access,* vol. 6, pp. 59728-59741, 2018.

[15]   J. You, Z. Fan, Y. Hu, and M. Deng, "Virtual resistor based DBVC and active damping method for DC bus stabilization of cascaded power converters system," in *2017 IEEE Transportation Electrification Conference and Expo, Asia-Pacific (ITEC Asia-Pacific)*, 2017: IEEE, pp. 1-6.

[16]   X. Lu, K. Sun, J. M. Guerrero, J. C. Vasquez, L. Huang, and J. Wang, "Stability enhancement based on virtual impedance for DC microgrids with constant power loads," *IEEE Transactions on Smart Grid,* vol. 6, no. 6, pp. 2770-2783, 2015.

[17]   A. Rygg and M. Molinas, "Apparent impedance analysis: A small-signal method for stability analysis of power electronic-based systems," *IEEE Journal of Emerging and Selected Topics in Power Electronics,* vol. 5, no. 4, pp. 1474-1486, 2017.

[18]   L. Yushan, K. R. Vannorsdel, A. J. Zirger, M. Norris, and D. Maksimovic, "Current Mode Control for Boost Converters With Constant Power Loads," *IEEE Transactions on Circuits and Systems I: Regular Papers,* vol. 59, no. 1, pp. 198-206, 2012.

[19]   X. Zhi-yu, Y. You-ling, X. Wei-sheng, and W. Qi-di, "Controllability of nonisolated DC-DC converters with constant-power-load," in *Control and Decision Conference (CCDC), 2012 24th Chinese*, 23-25 May 2012 2012, pp. 669-673.

[20]   R. Gavagsaz-Ghoachani, L.-M. Saublet, M. Phattanasak, J.-P. Martin, B. Nahid-Mobarakeh, and S. Pierfederici, "Active stabilisation design of DC–DC converters with constant power load using a sampled discrete-time model: stability analysis and experimental verification," *IET Power Electronics,* vol. 11, no. 9, pp. 1519-1528, 2018.

[21] A. El Aroudi, D. Giaouris, H. Ho-Ching Iu, and I. A. Hiskens, "A Review on Stability Analysis Methods for Switching Mode Power Converters," *Emerging and Selected Topics in Circuits and Systems, IEEE Journal on,* vol. 5, no. 3, pp. 302-315, 2015.

[22] M. K. Zadeh, R. Gavagsaz-Ghoachani, S. Pierfederici, B. Nahid-Mobarakeh, and M. Molinas, "Stability analysis and dynamic performance evaluation of a power electronics-based DC distribution system with active stabilizer," *IEEE Journal of Emerging and Selected Topics in Power Electronics,* vol. 4, no. 1, pp. 93-102, 2015.

[23] L. Herrera, W. Zhang, and J. Wang, "Stability analysis and controller design of DC microgrids with constant power loads," *IEEE Transactions on Smart Grid,* vol. 8, no. 2, pp. 881-888, 2015.

[24] C. H. Rivetta, A. Emadi, G. A. Williamson, R. Jayabalan, and B. Fahimi, "Analysis and control of a buck DC-DC converter operating with constant power load in sea and undersea vehicles," *IEEE Transactions on Industry Applications,* vol. 42, no. 2, pp. 559-572, 2006.

[25] D. Weijing, Z. Junming, Z. Yang, Q. Zhaoming, and P. Fangzheng, "Large signal stability analysis based on gyrator model with constant power load," in *Power and Energy Society General Meeting, 2011 IEEE,* 24-29 July 2011 2011, pp. 1-8.

[26] A. Griffo, J. Wang, and D. Howe, "Large signal stability analysis of DC power systems with constant power loads," in *Vehicle Power and Propulsion Conference, 2008. VPPC '08. IEEE,* 3-5 Sept. 2008 2008, pp. 1-6.

[27] J. Wu and Y. Lu, "Adaptive Backstepping Sliding Mode Control for Boost Converter With Constant Power Load," *IEEE Access,* vol. 7, pp. 50797-50807, 2019.

[28] X. Xiaoling, C. K. Tse, and R. Xinbo, "Bifurcation Analysis of Standalone Photovoltaic-Battery Hybrid Power System," *IEEE Transactions on Circuits and Systems I: Regular Papers,* vol. 60, no. 5, pp. 1354-1365, 2013.

[29] M. Huang, H. Ji, J. Sun, L. Wei, and X. Zha, "Bifurcation-based stability analysis of photovoltaic-battery hybrid power system," *IEEE Journal of Emerging and Selected Topics in Power Electronics,* vol. 5, no. 3, pp. 1055-1067, 2017.

[30] H. Wu and V. Pickert, "Stability analysis and control of nonlinear phenomena in bidirectional boost converter based on the Monodromy matrix," presented at the Applied Power Electronics Conference and Exposition (APEC), 2014 Twenty-Ninth Annual IEEE, 16-20 March 2014, 2014.

[31] H. Wu, V. Pickert, D. Giaouris, and B. Ji, "Nonlinear Analysis and Control of Interleaved Boost Converter Using Real-Time Cycle to Cycle Variable Slope Compensation," *IEEE Transactions on Power Electronics,* vol. 32, no. 9, pp. 7256-7270, 2017.

[32] V. Grigore, J. Hatonen, J. Kyyra, and T. Suntio, "Dynamics of a buck converter with a constant power load," in *Power Electronics Specialists Conference, 1998. PESC 98 Record. 29th Annual IEEE,* 17-22 May 1998 1998, vol. 1, pp. 72-78 vol.1.

[33] R. I. Leine and H. Nijmeijer, *Dynamics and bifurcations of non-smooth mechanical systems.* Springer Science & Business Media, 2013.

[34] D. Giaouris, S. Banerjee, B. Zahawi, and V. Pickert, "Stability Analysis of the Continuous-Conduction-Mode Buck Converter Via Filippov's Method," *IEEE Transactions on Circuits and Systems I: Regular Papers,* vol. 55, no. 4, pp. 1084-1096, 2008.

[35] D. Giaouris, S. Maity, S. Banerjee, V. Pickert, and B. Zahawi, "Application of Filippov method for the analysis of subharmonic instability in dc–dc converters," *International Journal of Circuit Theory and Applications,* vol. 37, no. 8, pp. 899-919, 2009.

[36] H. Wu, V. Pickert, and D. Giaouris, "Nonlinear analysis for interleaved boost converters based on Monodromy matrix," in *Energy Conversion Congress and Exposition (ECCE), 2014 IEEE,* 14-18 Sept. 2014 2014, pp. 2511-2516.

[37] H. Sakurai and Y. Sugimoto, "Design of a current-mode, MOS, DC-DC buck converter with a quadratic slope compensation scheme," in *48th Midwest Symposium on Circuits and Systems, 2005.,* 7-10 Aug. 2005 2005, pp. 671-674 Vol. 1.

[38] H. Wu, V. Pickert, X. Deng, D. Giaouris, W. Li, and X. He, "Polynomial Curve Slope Compensation for Peak-Current-Mode-Controlled Power Converters," *IEEE Transactions on Industrial Electronics,* vol. 66, no. 1, pp. 470-481, 2019.

Haimeng Wu (M'10) received the B.Sc. degree in electrical engineering from Chongqing University, Chongqing, China, in 2008. He obtained postgraduate recommendation prize with 1st class scholarship to Zhejiang University and then he obtained the M.Sc. degree in power electronics from College of Electrical Engineering, Zhejiang University, Hangzhou, China, in 2011. After receiving the scholarship from Engineering and Physical Science Council (EPSRC), he studied at Newcastle University in the UK. In 2016, he was awarded the Ph.D. degree in power electronics at the School of Engineering, Newcastle University, United Kingdom.

Dr.Wu joined in Electrical Power Research Group at Newcastle University as a Postdoctoral Researcher since 2015. In 2019, he was appointed as a Lecturer in the Department of Mathematics, Physics and Electrical Engineering, Northumbria University, UK. He is the winner of Siemens European TAPAS Community Challenge Competition 2018. His current research interests include power electronics for electric vehicles, health management of wide band gap (WBG) device and wireless power transfer.

Volker Pickert (M'04) studied at the RWTH Aachen, Germany, and Cambridge University, UK, and he received his Dipl.-Ing. degree in Electrical and Electronic Engineering from RWTH Aachen in 1994. He was awarded the Ph.D. degree in power electronics from Newcastle University, Newcastle upon Tyne, U.K., in 1997. From 1998 to 1999, he was an Application Engineer with Semikron GmbH, Nuremberg, Germany, and from 1999 to 2003 he was Group Leader at Volkswagen AG, Wolfsburg, Germany, responsible for the development of electric drives for electric vehicles. In 2003, he was appointed as a Senior Lecturer in the Electrical Power Group, Newcastle University, and in 2011 he became a Full Professor of Power Electronics. In 2012, he became the Head of the Electrical Power Group. He has published more than 200 book chapters, journal articles, and conference papers in the area of power electronics and electric drives. His current research interests include power electronics for transport applications, thermal management, health monitoring techniques, and advanced nonlinear control. Prof. Pickert received the IMarEST Denny Medal for the best article in the Journal of Marine Engineering in 2011 and in 2018 he received the Best Paper Award at IEEE International Conference on Computing Electronics & Communications Engineering (iCCECE), Essex, UK. He is regularly invited as keynote speaker and advises various governments on energy and transport related issues. In 2019, he also became Director of UK's EPSRC Doctoral Training Centre in Power Electronics for Sustainable Electric Propulsion. He is the active Editor-in-Chief of the IET Power Electronics journal.

Mingyao Ma (M'11) received the B.Sc. and Ph.D. degrees in applied power electronics and electrical engineering from Zhejiang University, Hangzhou, China, in 2004 and 2010, respectively. From October 2008 to October 2009, she was a visiting PhD postgraduate research student in the University of Strathclyde, Glasgow, U.K., and in 2010, she joined Zhejiang University as a Post-Doctoral Research Fellow. In 2011, she worked for the University of Central Florida, Orlando, US, as the visiting scholar. From April 2012 to April 2015, she joined the Newcastle University, Newcastle, UK, as the Research Associate. From 2015 she works in Hefei University of Technology as a professor. Her research interests include multilevel converters, distributed control of PEBB-based converters, software design using FPGA and DSP, SR motor control, and health monitoring and fault diagnostic technique of power electronics systems.
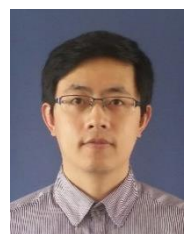
Bing Ji (M'13 - SM'18) received the BEng in Electrical Engineering and English as his double major from Dalian University of Technology, China, in 2004. He obtained MSc(Dist) and PhD in Power Electronics both from Newcastle University, U.K., in 2007 and 2012, respectively. He has undertaken different research roles in industry and academia since 2012. He joined the University of Leicester in 2015 as a lecturer of Electrical Power Engineering. His research interests include reliable power semiconductor devices and

modules, batteries and converters, intelligent gate drivers, thermal management, virtual prototyping, and high power-density converters in electric vehicle and aerospace applications. He is also a member of the IET and editor of IET Power Electronics Journal.

Chenming Zhang received the B.Eng. degree in automation from Hefei University of Technology, Hefei, China, in 2008 and the M.Sc degree in automation and control in 2014 from Newcastle University, Newcastle upon Tyne, United Kingdom.
He is currently pursuing the Ph.D. degree at the Department of Electrical and Electronic Engineering, Newcastle University. His research interests include control of modular multilevel converters (MMC), condition monitoring of power devices and wireless power transmission.